High-Resolution Aeromagnetic data for structural features mapping in the Mandjap I area, Douala-Cameroon: Implications for structurally-controlled Mineralization Prospection

Mono Jean Aimé[1*], Zanga Amougou Alain[2], Enyegue A Nyam Françoise Martine[3], Bouba Apollinaire[4] and Ndougsa Mbarga Théophile[5]

1. Department of Basical Science, Advanced Technical Teacher's Training College (ENSET), University of Douala, P.O. Box: 1872, Douala, CAMEROON
2. Department of Physics, Faculty of Sciences, University of Douala, Douala, CAMEROON
3. Department of Physics, Faculty of Sciences, University of Yaoundé I P.O. Box 812 Yaoundé, CAMEROON
4. Department of Physics, Higher Teacher's Training College (ENS), University of Maroua, CAMEROON
5. Department of Physics, Higher Teacher's Training College, University of Yaoundé I, P.O. Box 47 Yaoundé, CAMEROON
*monojeanaime@yahoo.fr

Abstract

A high-resolution aeromagnetic survey was conducted in the Mandjap I area, situated in the Pan-African zone (Douala-Cameroon). Various techniques including first vertical derivative, second vertical derivative, upward extension, signal analysis, spectral analysis and Euler deconvolution, were employed to highlight the different geological structures such as faults that could potentially host mineralization in the study area. The study area's fault system responsible for structuring was revealed through the current study which reveal a new magnetic-derived structural features with a high mineral prospection interest.

Based on qualitative and quantitative analysis of the aeromagnetic lineaments, the main identified directions in our study area are: ENE-WSW, NE-SW, E-W and N-S, with depths ranging from 78.55 to 287.86 m according to Euler deconvolution. These preferential directions are consistent with the directions of the great Pan-African tectonic structures of Cameroon. Furthermore, based on spectral analysis, the calculated depth of magnetic sources ranges from 0.258 km for shallow sources to 0.542 km for deep sources, indicating a shallow magnetic basement.

Keywords: Aero-magnetic data, Structural features, Mineral prospecting, Douala-Cameroon.

Introduction

The Mandjap I region, situated in southwestern Cameroon, constitutes an integral part of the Pan-African Central African chain. This chain is a geologically complex region, characterised by a rich tectonic history that has yet to be fully elucidated. The North Equatorial Pan-African Chain in Cameroon is characterised by Middle Neoproterozoic meta-sedimentary terrains, cut by Upper Neoproterozoic volcano-sedimentary and volcanic formations[34]. The region has been affected by several tectonic episodes including movements along major faults. These structures have played a crucial role in the emplacement and preservation of certain mineralizations in the study area.

Despite the numerous studies that have been conducted in this area, the structural framework remains poorly understood due to the lack of surface and subsurface data. That is why the use of geophysical techniques such as aeromagnetism is crucial to identify the shallow and superficial geological structures that control mineralization. This technique enables the identification of complex geological structures including faults and fracture zones that are not visible at the surface but play a key role in the distribution of mineralization[10]. Several authors have used the magnetic method to delineate zones of mineralization[1,3-5,20,45].

The magnetic method is based on the magnetic susceptibility of iron minerals present in rocks. Iron ores, such as magnetite and hematite, have higher magnetic properties than other rocks. By measuring and mapping these magnetic variations, it is possible to identify iron-rich zones and delineate associated geological structures[10]. High-resolution aeromagnetic data play an essential role in this process. These data provide a detailed picture of the subsurface, enabling the visualization of magnetic anomalies and the inference of information on geology and mineralization. The observation of aeromagnetic anomalies alone is insufficient for the deciphering of geological subtleties.

In order to obtain accurate and reliable results, various mathematical filters are applied to aeromagnetic data to highlight the geological structures that control mineralization. For instance, the calculation of vertical and horizontal derivatives facilitates the delineation of shallow magnetic sources while analytical signal analysis enables the identification of geological boundaries[43]. Tools such as the power spectrum and Euler deconvolution are employed to estimate the depth of magnetic sources, thereby furnishing valuable information on the geometry of potential mineralization zones[14,47]. In Cameroon, in the 1970s, over 150,000 km of flight lines spaced 0.75 to 1 km apart were flown by Canada as part of the Aeromagnetic

**** Author for Correspondence***

Reconnaissance Survey. These irregular surveys cover only about a third of the country. The data derived from these surveys have only provided a description of the regional geology of the areas covered. In recent years, the Cameroon Ministry of Mines, Industry and Technological Development (MINIMIDT) has organized a number of aeromagnetic surveys by national and international mining companies, with a view to mineral exploration.

The high-resolution airborne magnetic data used in this study came from one of these campaigns. They were acquired in February 2012 by the South African company Xplorer on behalf of Compagnie Minière du Cameroun (CMC) SA as part of Geotech's exploration work. The aim of this study is to characterize and to map the structural features to host potential mineralization in the Mandjap 1 area. To achieve this, we will use first vertical derivative (FVD), analytical signal (AS), 3D Euler deconvolution and spectral analysis methods on RTE aeromagnetic data covering the Mandjap I area and its surroundings.

Study area geological setting

Mandjap I region is located in central-western Cameroon (Figure 1). The study area is characterized by an equatorial climate, abundant rainfall and altitudes ranging from 84 to 895 meters (Figure 2). The region is geographically bounded by the coordinates presented in table 1. In Cameroon, the basement is typically composed of rocks from various Precambrian periods. In the southern region, this Precambrian basement consists of three primary geotectonic units. The Central African Pan-African Chain or Oubanguide Complex[36] is located in the north while the Yaoundé Group[33] is represented in the south.

The Ntem complex forms the northwestern boundary of the Congo craton[27] (Figure 1). The Mandjap I region and surrounding area are part of the Nyong complex, which is located between the Sanaga River to the north[49] and the Ntem complex to the south. This fragment describes a Cameroonian Paleoproterozoic unit that is part of the Pan-African Chain of Central Africa. The unit records the Eburnian orogeny that occurred during the collision between the Congo and Sao Francisco shields [9,12,26,37]. The lithostructural unit reworked during the Pan-African orogeny associated with the collision between the Congolese, West African and Saharan shields is still referred to as the North Equatorial Pan-African Chain (NEPC)[2,9,33,35,44].

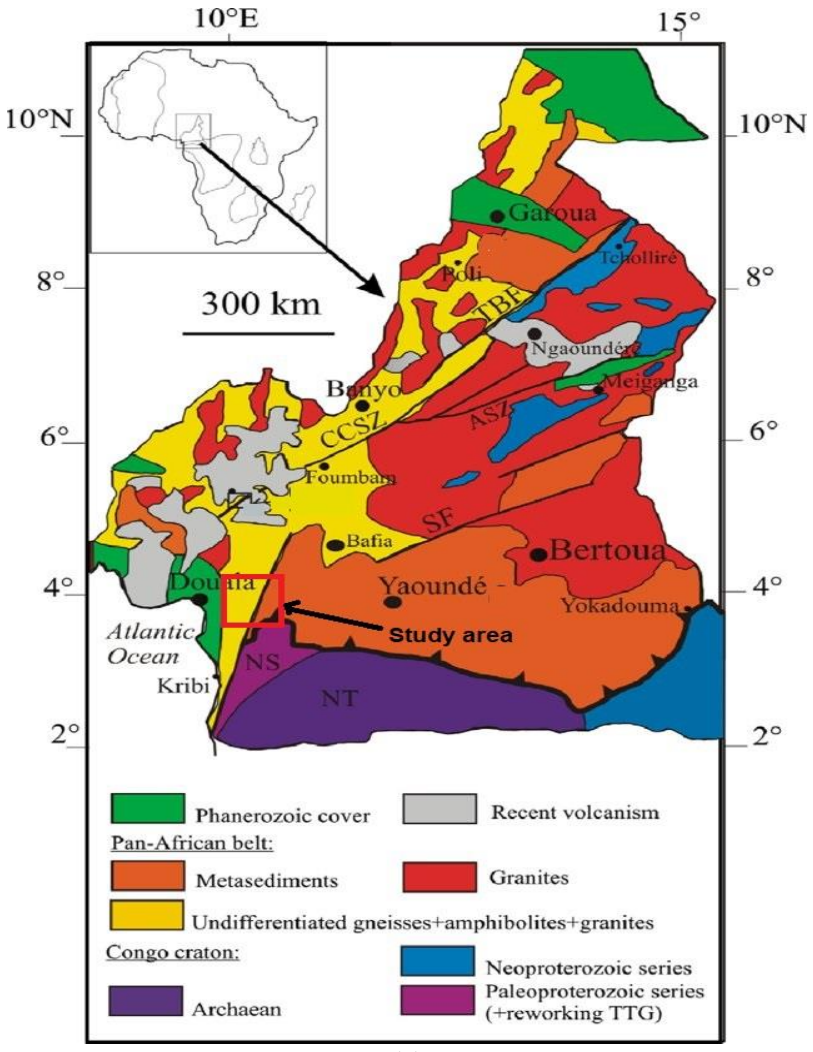

(a)

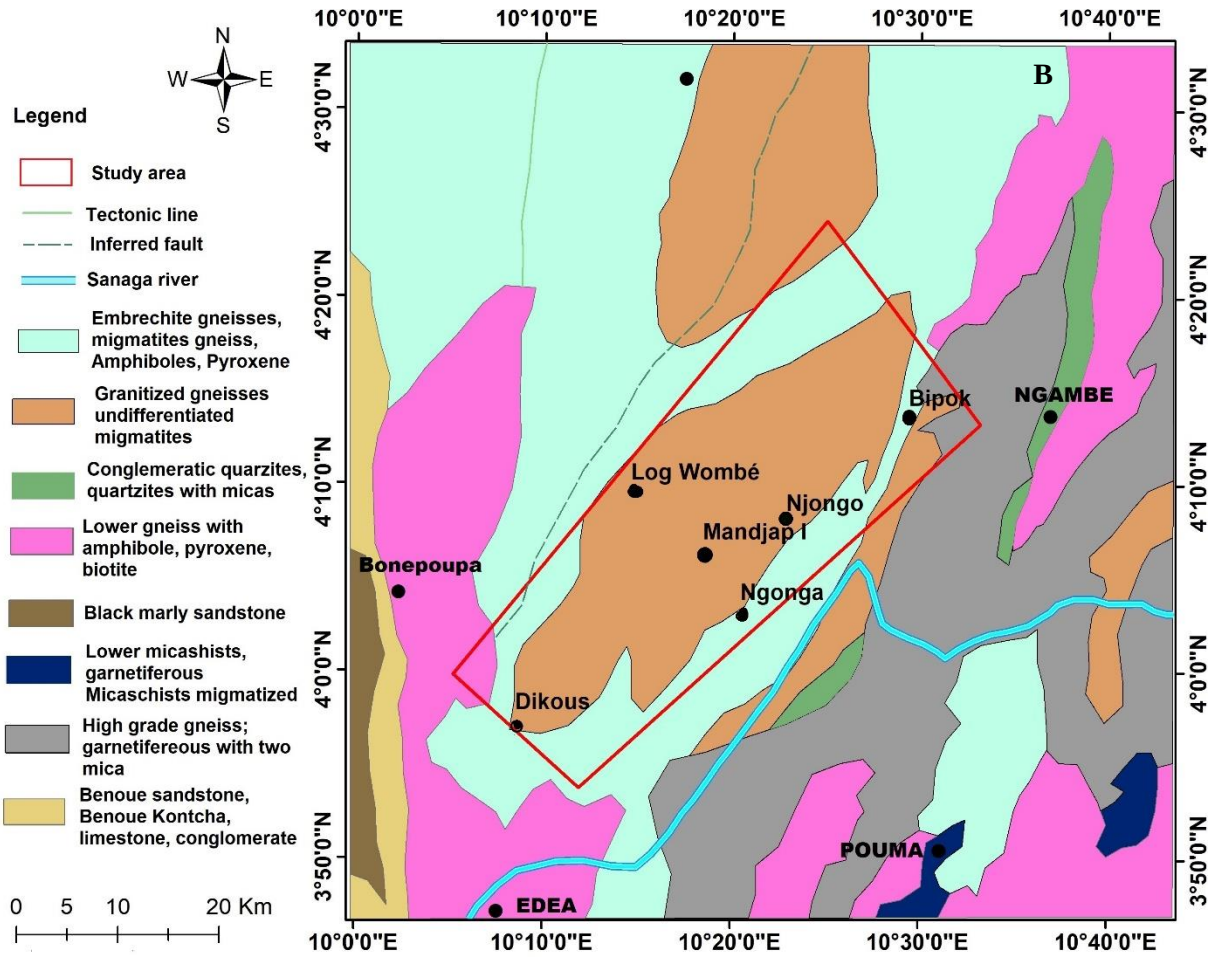

(b)

Figure 1: (A) Geological map of Cameroon, showing the major lithotectonic domains; ASZ, Adamawa shear zone; SF, Sanaga fault; TBF, Tcholliré-Banyo fault; CCSZ, Central Cameroon shear zone; NT, Ntem complex; DS, Dja group; NS, Nyong group[47]; (B) Geology map of study area

Table 1
Survey boundary coordinates

S.N.	X	Y	Long	Lat
1	-45490	443171	10.091957	3.994686
2	-9064	486806	10.416670	4.390074
3	5734	468024	10.550613	4.221479
4	-32020	434254	10.213327	3.915018

The Nyong complex is composed of metasedimentary and metavolcanic rocks, granitoids and syn-tectonic to late-tectonic syenites[24,38]. Nabighian et al[24] identified three distinct rock units within the complex: a unit of metasedimentary rocks (schists, garnet-rich micaschists). The text describes a unit of meta-igneous rocks including pyroxene-rich gneiss, garnet-rich charnockitic gneiss, charnockitic gneiss, biotite-rich gneiss, amphibole- and biotite-rich gneiss, garnet- and amphibole-rich gneiss, amphibolite, pyribolite, pyrigarnite and garnet-rich amphibolite. Additionally, it mentions a unit of melting rocks specifically migmatite and TTG, which exhibit quartzo-feldspathic segregation resulting from either *in situ* partial melting or injection along dykes or ductile shear zones. Structurally, the Nyong complex is dominated by a NNE break and has undergone a polyphase tectonic evolution[32]. The metasedimentary rocks exhibit a subvertical composite foliation ($S_{1/2}$), characterized by alternating ferromagnesian and leucocratic layers[12]. The meta-granitoids exhibit the S2 foliation. The entire Nyong complex is divided by NE-trending blastomylonite shear zones[36].

Material and Methods

Aeromagnetic data: The aeromagnetic data used in this study were obtained from a measurement campaign conducted in February 2012 by the South African company Xplorer on behalf of Compagnie Minière du Cameroun (CMC) SA as part of Geotech's exploration work. A 3 × Scintrex CS-3 cesium vapor magnetometer was used to

measure magnetic field intensity. The flight parameters were as follows: flight line spacing of 0.5 km, terrain clearance of 80 m, NW-SE flight lines, tie-line spacing of 2 km and NE-SW tie-line direction. The flight was conducted perpendicular to the general geological strike of the field, as indicated by Pouclet et al[39].

Methods: To aid in the interpretation of aeromagnetic data, various operators have been utilized. These operators are defined in the frequency domain using the Fourier transform and then transformed back to the spatial domain using the inverse Fourier transform. These processing operators and their comprehensive study have been made by various authors[6,22,23].

Reduced to Equator Magnetics (RTE): Aeromagnetic surveys conducted far from the magnetic poles may distort local magnetic anomalies due to the angle of the global magnetic field. This can make it difficult to interpret the magnetic data, as the magnetic anomaly may present a signal whose maximum or minimum is not generally vertical to the causative source. To accurately locate the magnetic anomaly's source, a procedure called 'Reduction to Pole' or (RTP) is applied. RTP is used to address this issue.

Reduction to pole is a mathematical function applied to the total magnetic field data in the frequency domain. The resulting product is the equivalent total magnetic field situated at the magnetic pole, thereby replacing the dipolar magnetic response with a simple peak positioned above the magnetic source.

The following equation describes the filter:

$$L(\theta) = \frac{1}{[sinI_a + icosI.\cos(D-\theta)]^2} \quad (1)$$

where I = Inclination of magnetic field, Ia = Inclination for amplitude correction and D = Geomagnetic declination.

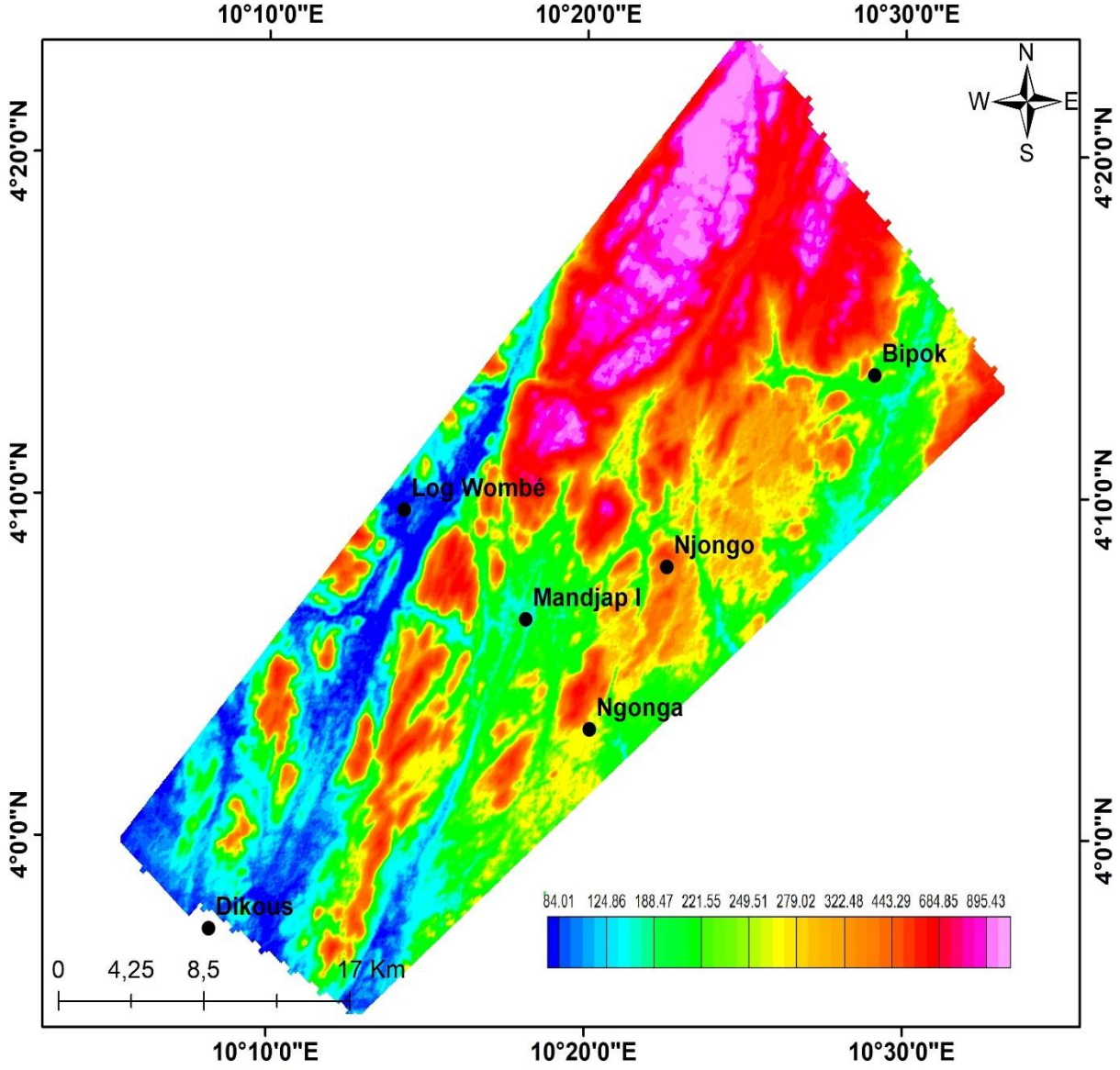

Figure 2: The digital elevation model of the study area, showing elevation values in meter

In low-latitude regions such as the one discussed here, RTP can cause distortion by amplifying N-S directions. To address this issue, Reduction to Equatorial (RTE) is applied[18]. The reduced field expression at the equator is given by the following relationship [19]:

$$L(\theta) = \frac{[sinI - icosIcos(D-\theta)]^2 \times (-cos^2(D-\theta))}{[sin^2Ia + cos^2Ia.cos^2(D-\theta)] \times [sin^2I + cos^2Icos^2(D-\theta)]} \quad (2)$$

If $(/Ia/</I/), Ia = I$

where I = geomagnetic inclination, Ia = Inclination for amplitude correction (never less than I), D = geomagnetic declination, L(θ) is Reduction to Equator and θ is the wave number direction.

Analytical Signal (AS): The analytic signal (AS) is a combination of the derivatives of the total magnetic field or the square-root of the sum of the square of derivatives of the total magnetic field[43]:

$$AS(x,y,z) = \sqrt{\frac{\partial T}{\partial x} + \frac{\partial T}{\partial y} + \frac{\partial T}{\partial z}} \quad (3)$$

The advantage of utilizing the analytic signal (AS) is that AS highs are directly over causative magnetic sources, regardless of geometry or remnant magnetic effects. The AS is useful in identifying the boundaries of magnetic source bodies, especially in cases where remanence and/or low magnetic latitude complicates interpretation[6,43]. However, since the AS is a derivative filter, deeper information is lost and the filter accentuates shallower features. In other words, the filter emphasizes surface-level characteristics while neglecting those that are deeper or have longer wavelengths. The strength of the analytic signal anomaly is directly related to the magnetic susceptibility of the causative body. This means that the greater is the proportion of magnetic minerals in the body, the larger the anomaly will be.

Essentially, the analytic signal provides a map of the magnetite distribution in the shallow underlying geology. However, it is important to note that the analytic signal has a tendency to blur anomalies. The AS filter, which is sometimes stretched, is typically one of the primary tools used in combination with Spectrum EM data. The AS filter, which is sometimes stretched, is typically one of the primary tools used in combination with Spectrum EM data. This dataset is likely the most useful.

Derivative filters: Derivative-based filters are used to calculate magnetic data in either the space or frequency domains. They sharpen the edges of magnetic anomalies and determine their locations[21]. The horizontal derivative in the 'X' direction highlights lithological and structural contacts and tectonic faults perpendicular to the axis, which is north-south in this case. The 'Y' horizontal derivative highlights lithological contacts in an east-west direction. The calculation of the first and second vertical derivative (FDV and SVD) of the magnetic data can be performed in either space or frequency domains. This is a standard filter that accentuates shallow features and structures[23] and is also useful for discriminating textural changes that characterize different lithologies.

It is important to note that while SVD has greater resolving power than FDV, its application requires high-quality data [15] due to its tendency to enhance noise along with high-frequency signals. SVD has the unique characteristic of canceling out and rapidly changing sign at a point directly above a contact[50]. The quality of geophysical data can often be evaluated by generating first and second vertical derivatives.

Upward continuation: The upward continuation is a transformation that the potential field observed on a surface can undergo, to obtain the field that would be observed on a surface above that of initial observation. Applying this type of filter attenuates the short-wavelength magnetic variations attributable to surface sources, while enhancing the long-wavelength variations is attributable to deep sources [16]. In addition, the upward continuation makes it possible to see the theoretical evolution of anomalies and contacts at different depths [16], since the upward observation altitude of z meters corresponds in theory to the magnetic response of sources deeper than zo = z/2 meters.

Euler 3D Deconvolution: The Euler homogeneity equation is a mathematical procedure commonly used to locate and to determine magnetic and gravity source parameters in magnetic and gravity data interpretation[41,47]. Euler deconvolution is particularly effective in delineating contacts and rapidly assessing depth. Regnoult[41] provided the following representation of the Euler homogeneity equation:

$$\frac{\partial M}{\partial x}(x-x_0) + \frac{\partial M}{\partial y}(y-y_0) + \frac{\partial M}{\partial z}(z-z_0) = SI(B-M) \quad (4)$$

The detected effect is from the source located at (x_0, y_0, z_0), with M representing the total field and B representing the regional field. N, also known as the degree of homogeneity or structural index (SI), characterizes the source. The derivatives of the total field are represented by $\partial M/\partial x$, $\partial M/\partial y$ and $\partial M/\partial z$. For magnetic data. Spector and Grant[47] demonstrated that N ranges from 0 to 3, depending on the structure being considered: 0 for a contact, 1 for a dyke, 2 for a cylinder and 3 for a sphere. Regnoult[41] concluded that the best estimates of depths are provided by low structural indices ranging from 0 to 1.

Radially average power spectrum (RAPS) for depth estimation: Known as the "power spectrum curve", spectral analysis is a technique based on fast Fourier transform filtering. It represents the spectral energy distribution of data in terms of wave numbers[46]. Spectral analysis is applied in the interpretation of gravity and magnetic data to map the roof of the magnetic basement and to estimate the average

depth of all sources observed on a profile or anomaly map[15]. This method provides a representation (spectral curve) of potential anomalies as a function of their wavelength and amplitude. Typically, this spectral curve illustrates three characteristic parts:

- The first part, located in low frequencies, corresponds to deep structures;
- The second part, in the middle frequencies, corresponds to surface structures;
- The third part, at high frequencies, corresponds to noise.

From this representation, we can plot the slope of each of the right-hand segments of the equation that enables us to define the depth of the various geological units from the following equation[7]:

$$H = \frac{S}{4\pi} \quad (5)$$

where H is the depth and S the slope of the logarithmic spectrum (energy).

Results

Qualitative Interpretation: The map of total magnetic field anomalies (Figure 3a) displays variations caused by subsurface heterogeneities. The shape and amplitude of these anomalies differ depending on the depth, shape and magnetic susceptibility contrast of the geological formations in the study area. A visual analysis shows two zones of magnetic facies that are distinctly separated by visible boundaries. A large NE-SW-trending zone is generally characterized by a strong magnetic response. The area surrounding this zone exhibits a weak magnetic response with a few positive linear anomalies. However, the anomalies depicted on this map are not aligned with causal sources, as their shape and amplitude are influenced by changes in the tilt of the Earth's magnetic field. To vertically align the residual magnetic field anomalies in the investigation area with their causative sources, the RTE has been applied.

Figure 3b illustrates the RTE transformation which shows the sum of the effects of all magnetized bodies, regardless of their orientation, nature, or magnetization intensity. A visual analysis of this map reveals that the amplitudes of the Binga anomalies range from -763.16 nT to 763.33 nT, with dominance in the ENE-WSW direction. The shape, orientation and amplitude of these anomalies depend mainly on lithological and morphological variations in the underlying geological formations. Anomalies with negative intensity are highlighted in red and magenta while those with positive intensity are highlighted in light and dark blue, corresponding respectively to geological materials with low and high magnetic susceptibility. High-intensity positive anomalies are mainly located along the eastern boundary of the study area and they also appear in thin and elongated forms in the rest of the region. To the southwest of the study area, in and around the locality of Bikou, there is a significant northeast-southwest to northwest-southeast anomaly. The presence of a strong negative anomaly is highlighted to the northwest.

Derivative-based filters maps: The TMI-RTE map underwent processing with the First Vertical Derivative (FVD), Second Vertical Derivative (SVD) and horizontal gradients along X and Y to emphasize linear features such as fractures, faults and shear zones. Figures 4a, 4b, 5a, 5b and 6 display the horizontal derivative maps for 'X', 'Y', FVD, FVD-grey shaded and SVD respectively. A visual analysis of these maps reveals a series of linear magnetic features with preferential ENE-WSW and NE-SW directions. Compared to the horizontal derivative map along the Y-axis, we observe a difference in the intensity of magnetic anomalies on the horizontal gradient map along the X-axis (Figure 4a), reaching 1.0 nT/km. This map does not show any north-south orientation.

In contrast, the Y-axis horizontal gradient (Figure4b) highlights east-west contacts in the horizontal plane and reveals changes in the shape, intensity and direction of certain magnetic anomalies. Figure 5 highlights some E-W directions to the southwest of the study area, north of the Log Wembe locality and in the Bipok locality to the north of the region which were not shown on the previous map. The major ENE-WSW direction remains unchanged.

Vertical derivatives (FVD and SVD) are filters that enhance shallower geological anomalies[4]. This enhancement accentuates anomalies on bodies and tends to reduce anomaly complexity, resulting in a clearer picture of causal structures. The FVD map (Figure 5) illustrates well individualized, short-length magnetic responses which would be associated with superficial sources. Compared to the TMI-RTE map (Figure 4), the FVD map displays a noticeable difference, characterized by an enhanced visibility of structural features. The lineaments associated with magnetic contacts are mapped through a straightforward application of the first-order vertical derivative. To better emphasize the structural directions highlighted on the vertical gradient map, a shaded relief map (Figure 5b) of the FVD was generated. The map visually represents the complexity of the studied area by highlighting the various fracturing and contact lines in the base.

The SVD map in figure 6 shows clearly the limits of shallow anomalies. The second vertical derivative map reveals the limits of the shallow anomalies, allowing for the delineation of possible mineralization zones. The SVD map produced reinforced subtle anomalies while reducing regional trends. It accentuated near-surface effect anomaly boundaries and defined causal body edges in the study area. Additionally, it amplified structure, lineament and fault trends (Figure 6), with the longest northeast-southwest-trending fault suspected to be a paleostructure.

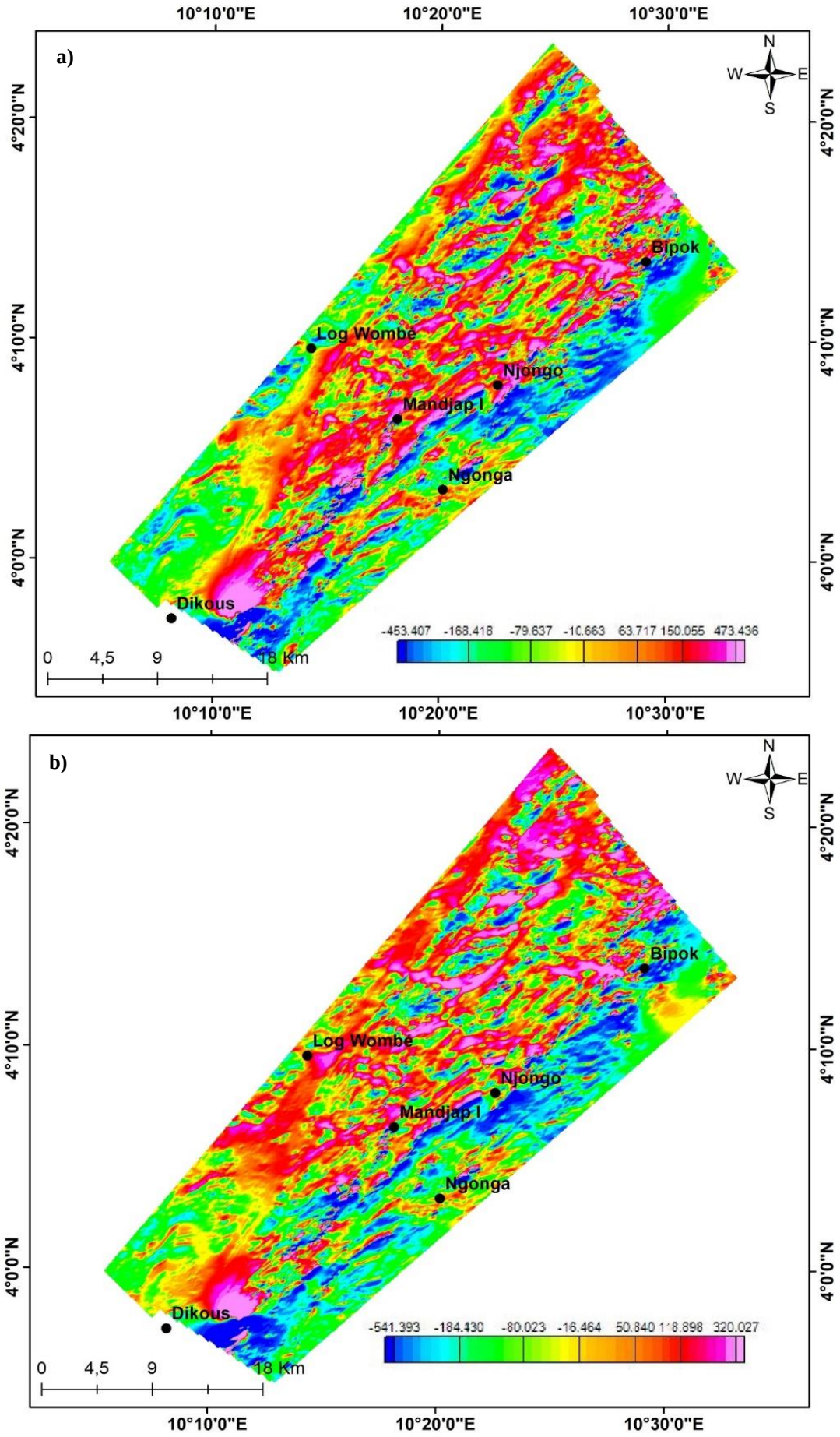

Figure 3: (a) Total Magnetic Intensity (TMI) and TMI Reduce to Equator (TMI-RTE) (b) maps

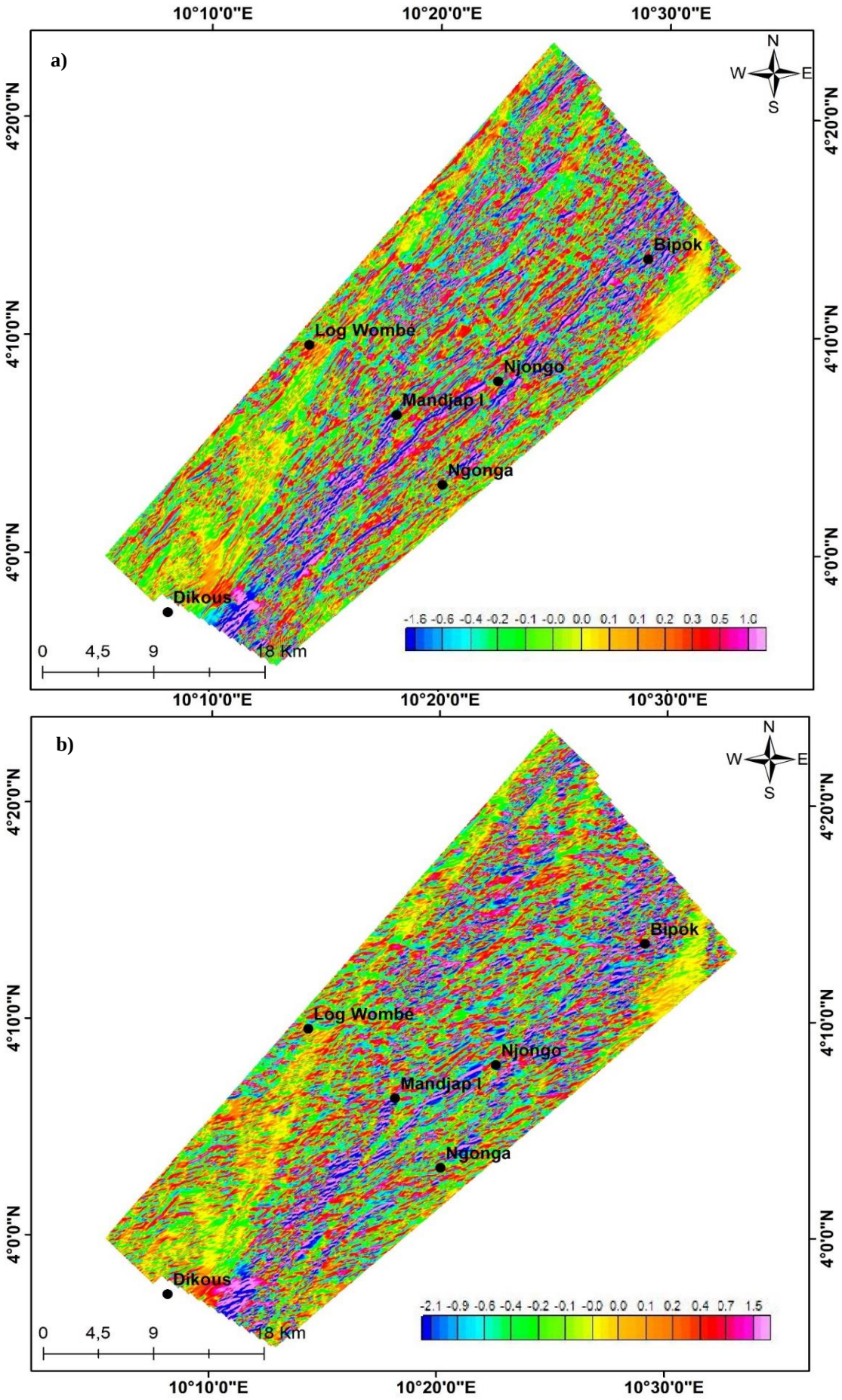

Figure 4: (a) Horizontal Derivative (in x- direction) and Horizontal Derivative (in y- direction) (b) maps

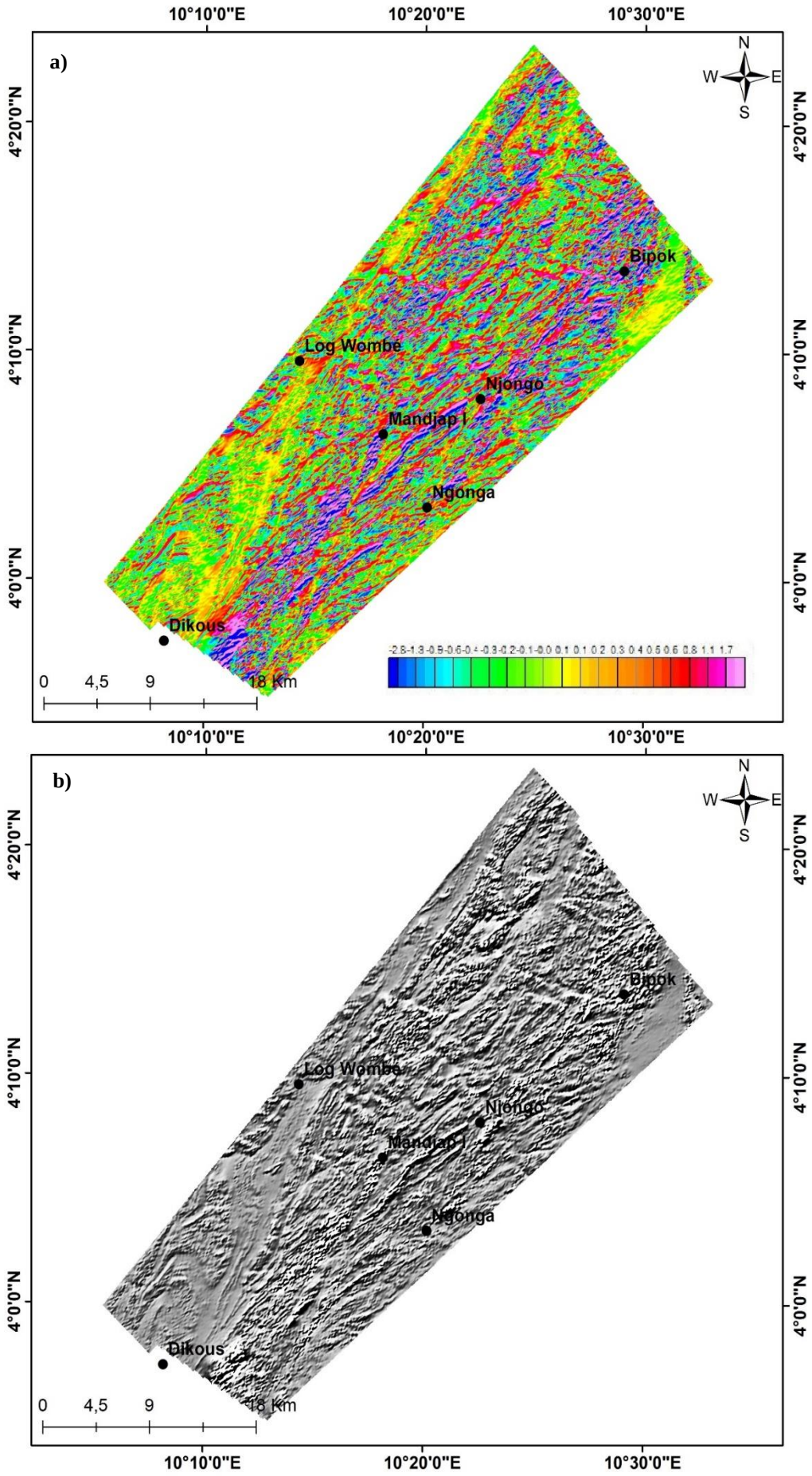

Figure 5: (a) First Vertical Derivative and FVD grey shaded (b) maps

Analytical Signal (AS): Although AS has limited use for source modelling, it can locate the position of sources in the horizontal plane, regardless of whether the magnetization is remanent or induced[6,43]. Figure 7 shows the map of the analytical signal amplitude, which highlights the major tectonic directions and helps to limit contacts between geological formations with strong magnetizations due to their susceptibility contrasts and to expose intrusive bodies[25]. The analytical signal maps (Figure 7a) illustrate anomalies with amplitudes ranging from 0.1 to 3.8 nT. Linear and subcircular anomalies with high intensities are visible, indicating the boundaries of intrusive bodies and strongly magnetic linear structures. Figure 7 highlights these structures.

Linear structures are concentrated at Mandjap I, south of Mandjap I, Ngonga, Djongo and north of Djongo. The major directions (ENE-WSW and NE-SW) highlighted on the vertical gradient maps and the horizontal gradients along X and Y are well represented on the AS map. Zones with amplitudes greater than 0.106 may indicate later tectonic activity where magma penetrated pre-existing rocks and solidified in fractures, faults and joints resulting from earlier tectonic activity.

Upward continuation: The upward extension is equivalent to a low-pass filter, attenuating the high frequencies of magnetic anomalies associated with the effects of surface magnetic structures, leaving only the effects of deeper structures visible. Figures 8a to 8d show the TMI-RTE maps of the study area, extended to altitudes of 1 km, 2 km, 3 km and 4 km respectively. According to Hinze et al[16], this transformation concentrates the subsurface response at the following minimum depths: 0.5, 1, 1.5 and 2 km. Thus, TMI-RTE composite images at various upward extension altitudes (Figure 8) show that the impact of surface structures is reduced, or even eliminated, while anomalies generated by deeper sources are accentuated. There is a very significant filtering effect on magnetic signatures for the 1 km extension (Figure 8a).

The short-wavelength anomalies present on the TMI-RTE are almost no longer visible and their disappearance confirms that they are linked to surface structures. They have given way to single, simple and regular anomalies, with a strong smoothing of the curves and a sharp drop in amplitudes. At 2 km (Figure 8b), the smoothing is much more pronounced and we still note the presence of large magnetic units (positive and negative) separated by a flexure.

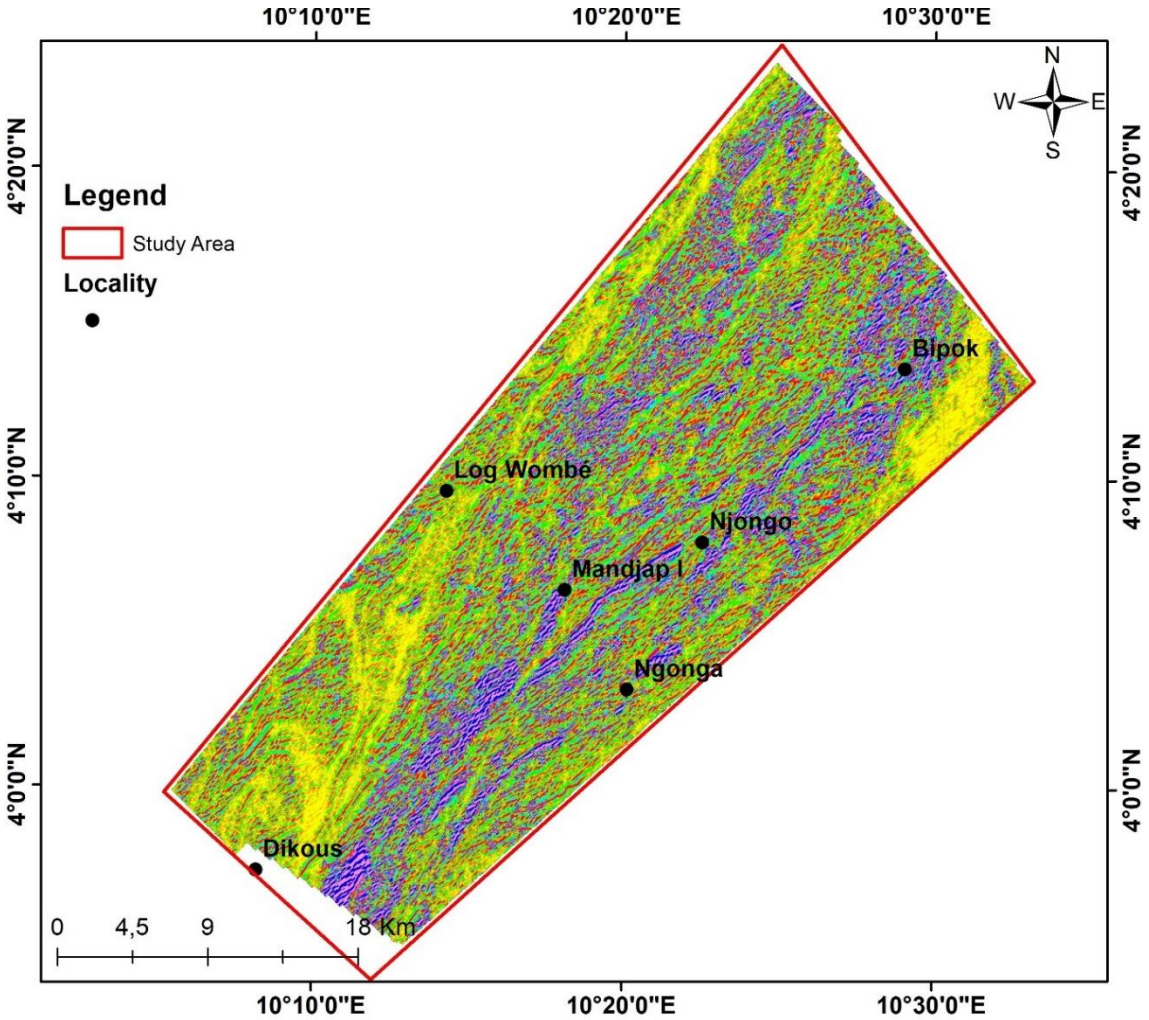

Figure 6: Second Vertical Derivative Map

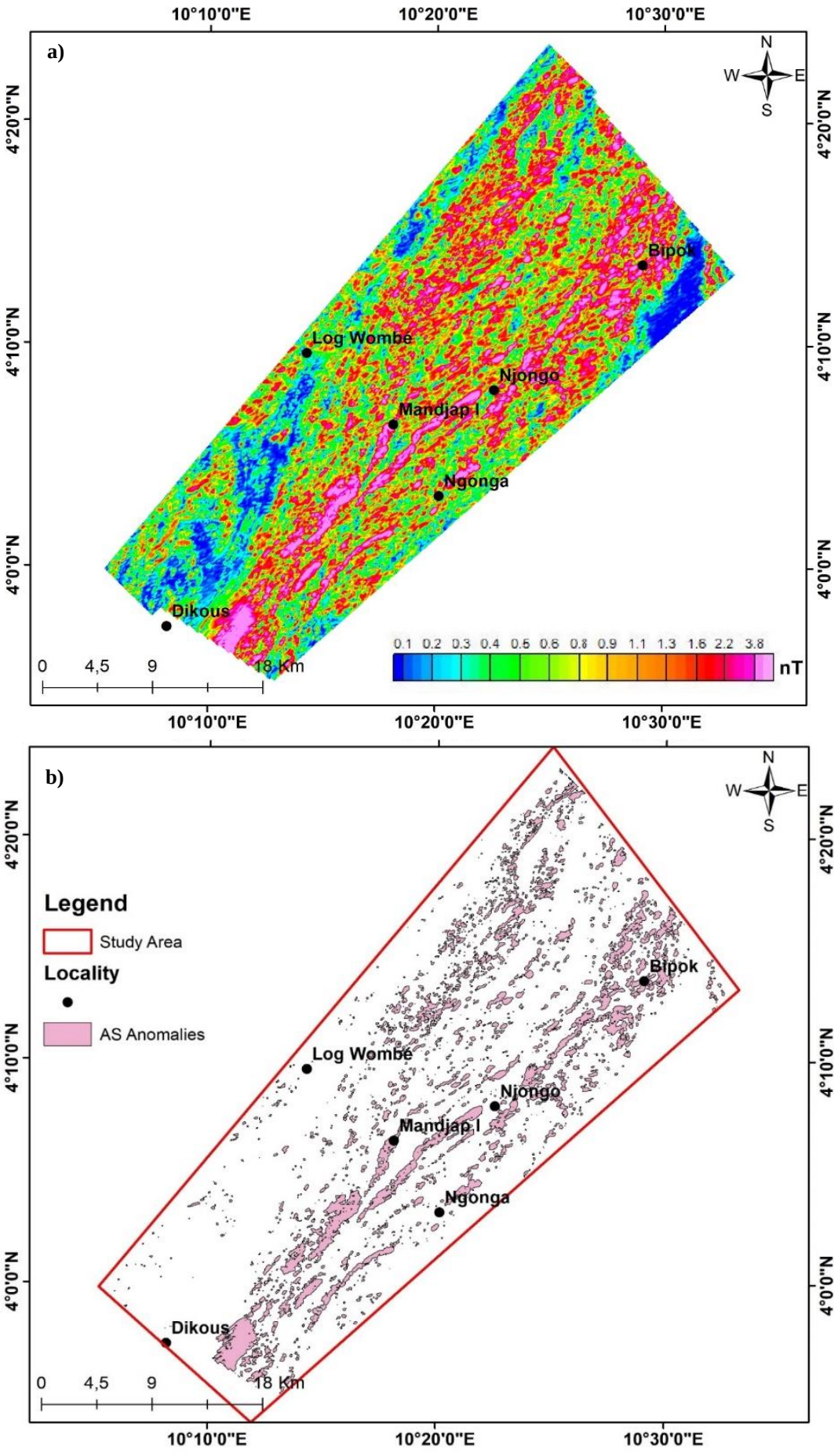

Figure 7: (a) Analytic signal and High anomalies Analytic signal (b) maps

This inflection would correspond to the response of a deep regional source. At 3 and 4 km (Figure 8c and 8d), virtually all are sets of anomalies characterized by long wavelengths linked to deep structures. These large ensembles are very distinct and highly differentiated in terms of amplitude. The upward extensions (Figure 8) express regional structural directions. The ENE-WSW direction, which extends from the Bipok region to Mandjap, corresponds to a deep-seated accident, as it persists on the extended maps.

Radially averaged power spectrum: Spectral analysis was used to estimate the mean depths of the magnetic sources in the Mandjap I area and its surroundings. The spectral curve analysis (Figure 9) revealed two distinct linear segments indicating that deep magnetic sources have wave numbers ranging from 0.00 to 0.357 cycles per k unit, which corresponds to an average depth of approximately 0.542 km. Superficial sources are associated with wave numbers ranging from 0.357 to 1.49 cycles per k unit, which corresponds to an average depth of approximately 0.258 km.

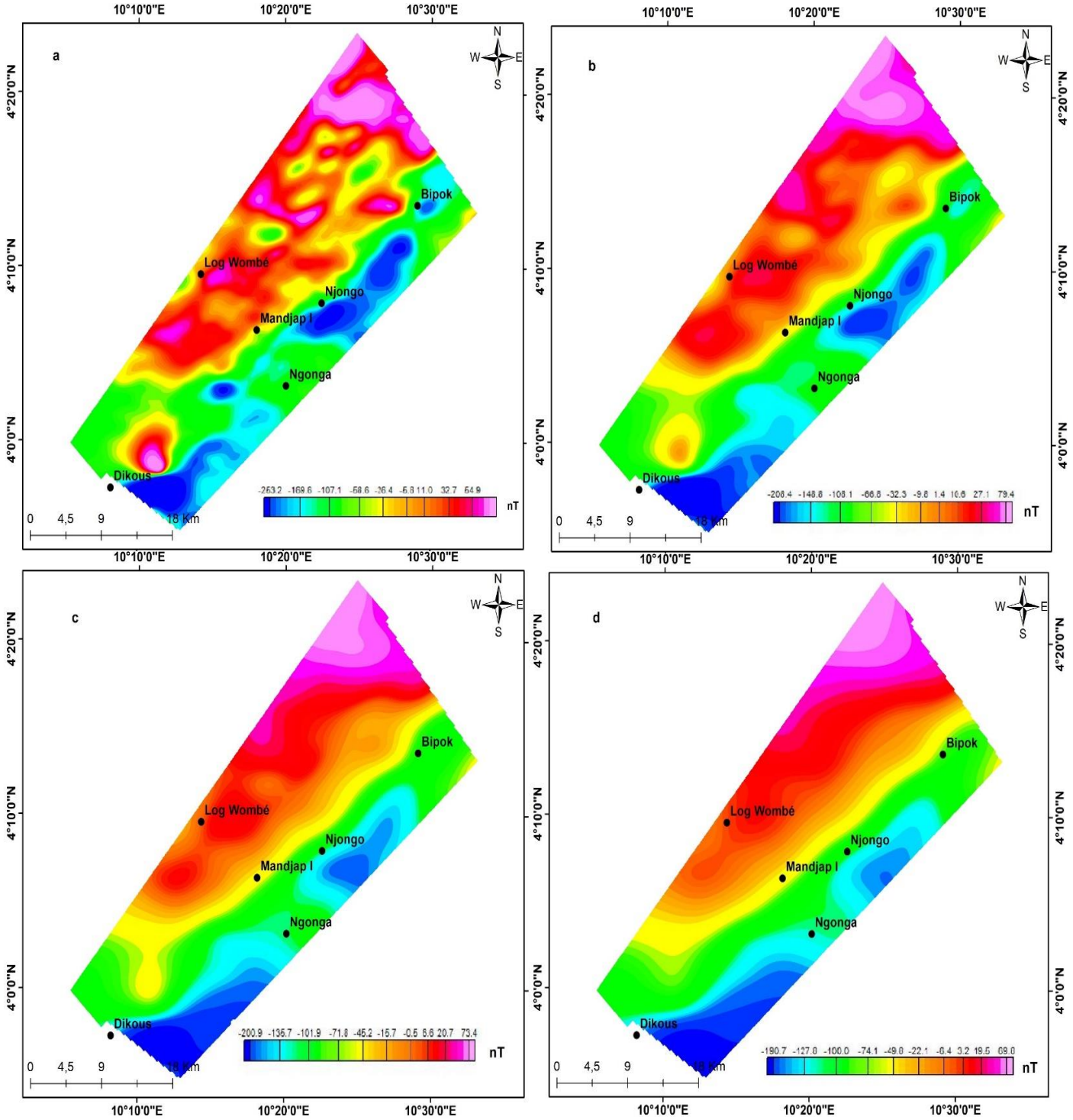

Figure 8: Upward continued map at (a) 1 km, (b) 2 km, (c) 3 km and (d) 4 km.

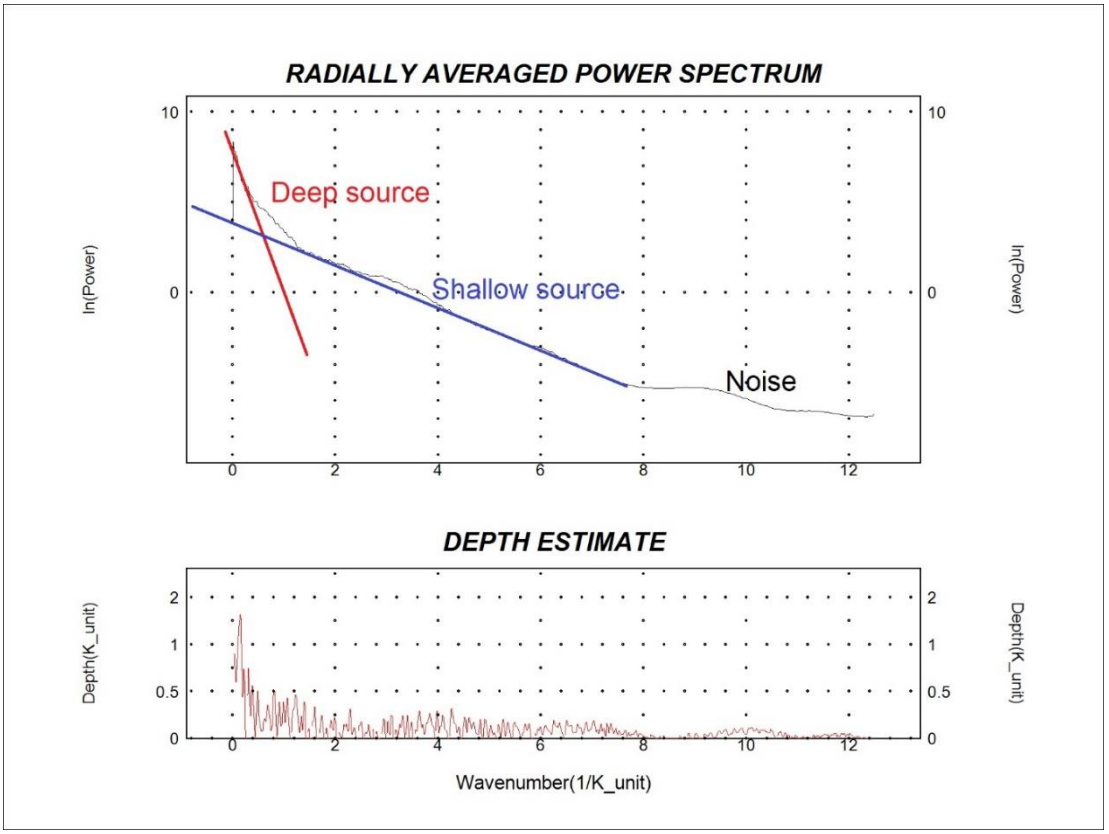

Figure 9: Radially Average Power Spectrum Analysis

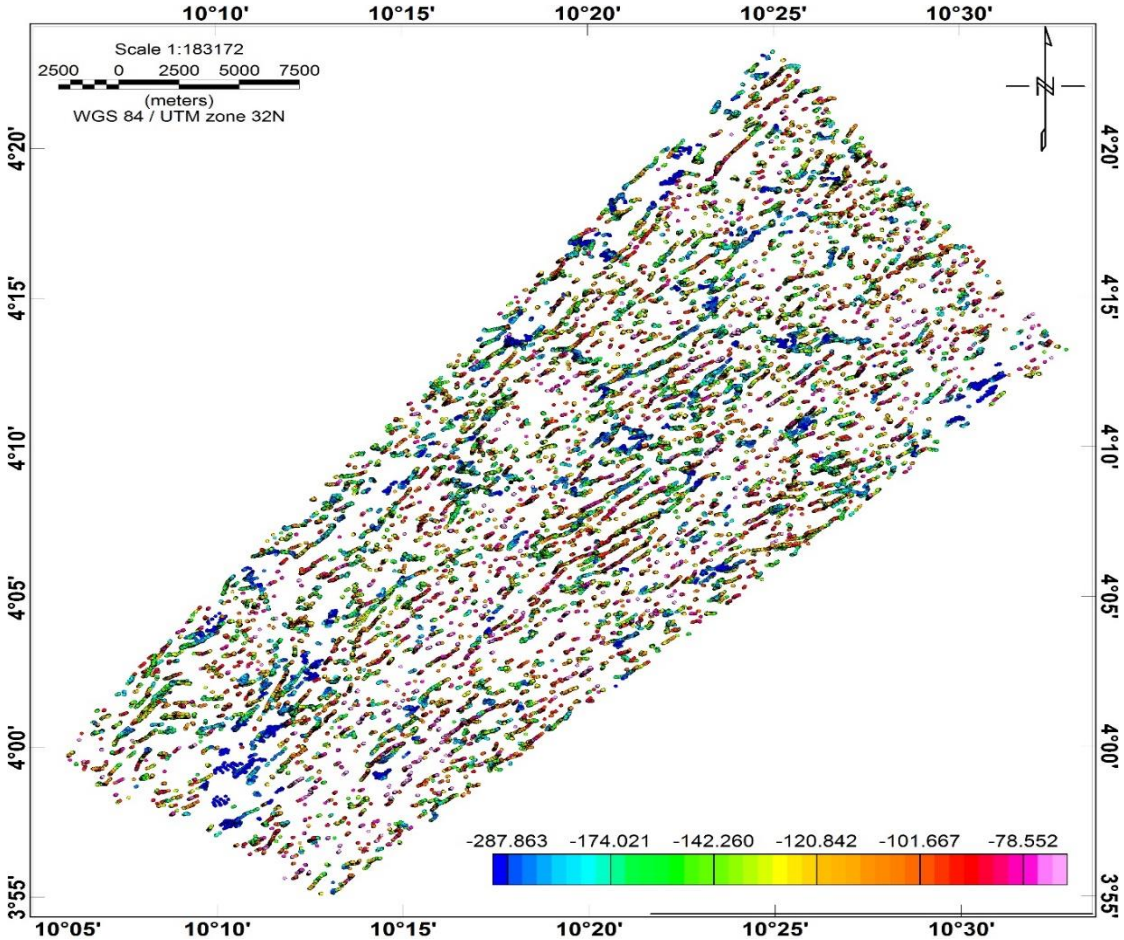

Figure 10: Euler solution map for the structural index N=1.0, 10×10 km window and a maximum relative error of 7 %.

Euler Deconvolution 3D: The study utilized a 3D Euler deconvolution method which is incorporated into Oasis montaj 8.4, to locate and to estimate the depth of magnetic sources. This method is highly efficient and requires little prior knowledge about the magnetization of causative sources. A 10 x 10 window, a structural index N = 1 and a tolerance of 7% were chosen for the TMI-RTE. The outcome of this technique is presented in Figure 10.

The analysis of the image shows that the depths of the solutions obtained range from 78.55 to 287.86 m. The main directional trends are ENE-WSW and NE-SW, which are highlighted in the map. The map also confirms the results obtained from FDV, SA, SDV and horizontal derivatives along X and Y, indicating the main fracturing directions in the study area

Structural map: To differentiate the tectonic trends that affect the Mandjap I region and its surrounding area, we have plotted the dominant magnetic discontinuities on the FVD, SVD, DX, DY, AS and Euler solution maps and presented them on the synthetic map in Figure 11a. This map highlights the various geological features that characterize the investigation area, identified as either faults or fractures. Accidental faults have long been suggested to interact with mineral deposits by providing pathways for concentrating mineralized fluids in the upper crust. They have also been used as a reference in exploration[14].

The synthetic map (Figure 11a) distinguishes between major and minor structures. Mandjap I and its environs comprise a total of 2843 lineaments with lengths ranging from 0.073 km to 21.237 km, totaling 1949.90 km with an average length of 0.684 km. The directional rosette in figure 11b shows that the main structural trends controlling the study area are ENE-WSW and NE-SW. The structural map was superimposed on the high-amplitude anomalies of the analytical signal to highlight potential mineralization zones.

Lineament density map: To determine the frequency of lineaments per unit area, we conducted a thorough analysis of lineament density. Lineament density serves as an indicator of the degree of fracturing in the rock. We identify areas with relatively high lineament density as zones of high rock fracturing, which are considered favorable for mineral exploration. Figure 11c shows the magnetic lineament density map, which displays very low-density linear structures (grey in color) located near the study area. The study area is almost entirely occupied by lime-green intermediate density zones which are surrounded by low-density lineament structures shown in blue.

High and very high lineament density structures, shown in orange and purple respectively, are found only as pockets within the intermediate density zones. High lineament densities are concentrated to the south of Mandjap I, with a NE-SW trend and are also found from the center to the north of the study area in the vicinity of Mandjap, Ngonga and Njongo. Very high lineament densities are found only to the south of Mandjap I, to the east of Dikous.

Discussion

As stated previously, the research findings are solely based on the analysis of magnetic data. The primary goal of the study is to identify and to map geological structures that could potentially contain mineral deposits. The TMI-RTE map was generated by vertically aligning the residual magnetic field anomalies of the study area using the RTE method to locate their causative sources. The interpretation of the TMI-RTE is qualitative and involves direct visual study of the magnetic signatures to extract geological information for preliminary interpretation. The TMI-RTE map of Mandjap I and its surroundings reveals a complex pattern of long- and short-wavelength magnetic signatures, as observed visually. The variable amplitude of anomaly signatures suggests different magnetic intensities from various sources. Negative anomalies are related to rocks, while positive anomalies correspond to basement rocks such as gneisses.

The TMI-RTE underwent filtering using FVD, SVD, DX and DY, resulting in 2847 lineaments. These lineaments were then categorized into first-order and second-order multidirectional fracture families of varying lengths, providing insight into their depth and structural significance (Figure 11a). The linear structures in the study area were grouped into four main classes based on their directional family. These classes follow particular preferential directions with different orders of magnitude, highlighting the geological heterogeneity of the area. This area is part of a regime of Riedel system structures[8,42]. The identified main directions, in order of priority, were determined through qualitative and quantitative analysis of the lineaments. ENE-WSW, NE-SW, E-W and N-S.

The study area is characterized by four main directions: The ENE-WSW direction is the most significant and corresponds to a series of intense shears accompanied by mantle uplift and granitization. This direction marks phase D3 and is the materialization of the mylonitic foliation (main dextral shear N070), grouping together shears also known as Central Cameroon Shear Zone (CCSZ), Sanaga Fault (SF) (FS) and Adamawa Fault (AF)[13,40]. The Pan-African tectonics on a regional scale is characterized by the ENE-WSW orientation which has been highlighted on Adamaoua structures[11,31].

he NE-SW structural direction observed here is believed to be the result of compressional forces acting along the NW-SE axis and accompanying regional metamorphism. The text is consistent with the transition zone between the Pan-African Range and the Congo Craton[29,48]. It characterizes the structures beneath the Craton in the study area. The NE-SW directions (D2) correspond to the secondary Riedel P-type structure, which are the lithological signatures of the regional schistosity[17].

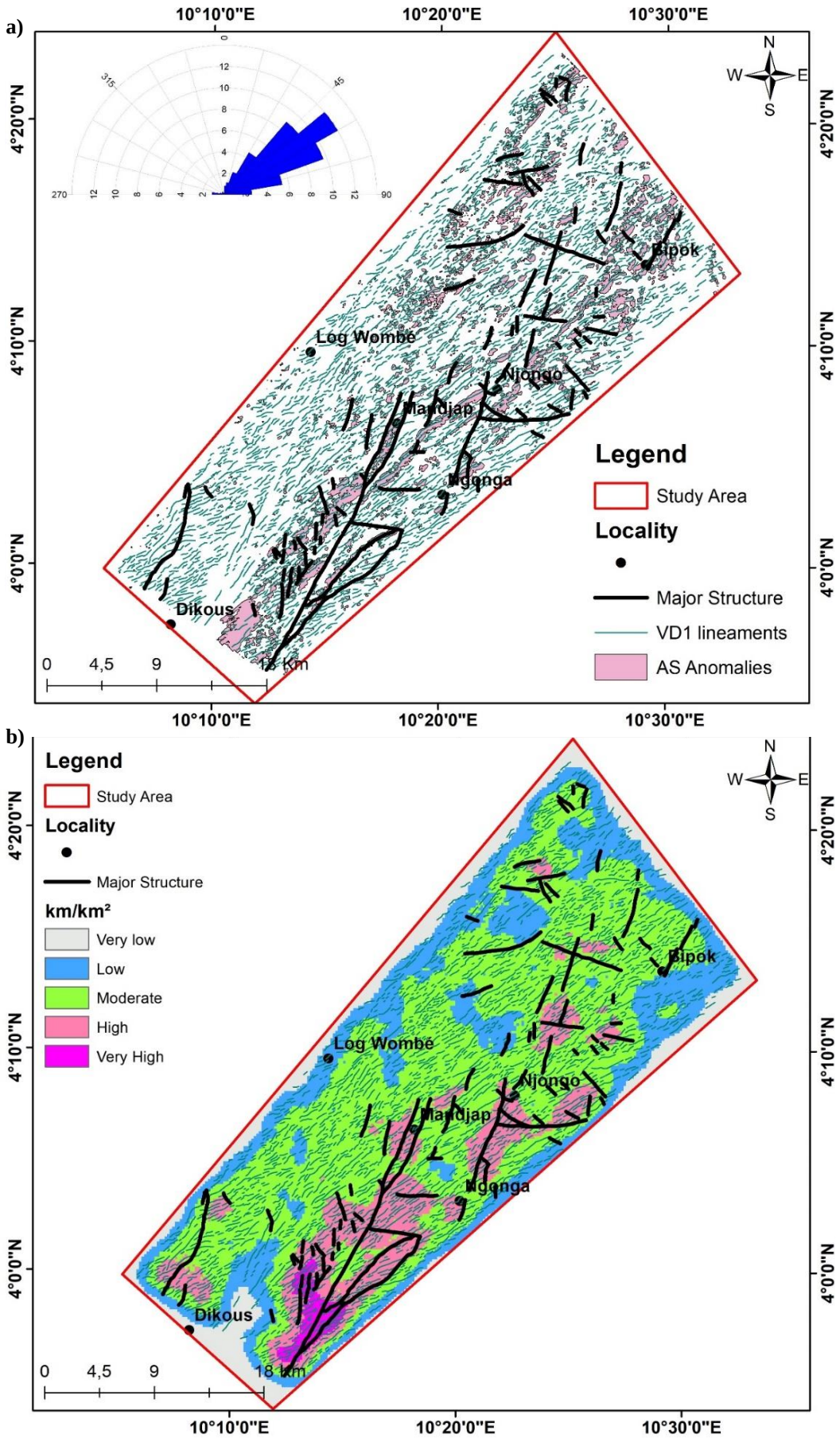

Figure 11: (a) Structural of aeromagnetic lineament map with the corresponding directional rose diagram. (b) Lineament density map

The NW-SE directions represent R' type Riedel structures. The secondary Riedel structures of type P' correspond to the N-S directions, while the Riedel structures of type R are represented by the E-W direction (D2). The E-W oriented lineaments reflect older structural trends that survived the Pan-African remobilization (600 Ma), indicating that the Precambrian rocks in this region endured rearrangements of 600 Ma.

Lineament density, expressed as the number of lineaments per unit area, was then calculated for the entire study area. This approach enables the identification of zones with more intense fracturing, which are considered as priority targets for mineral exploration. Indeed, according to Neves et al[28] areas of high lineament density are generally associated with greater permeability and fluid flow. The magnetic lineament density map reveals a heterogeneous distribution of linear structures in the study area. A number of distinct density classes can be identified, ranging from very low to very high, with varying characteristics. Zones of very low lineament density may indicate poorly fractured zones, which are less suitable for mineral exploration. Zones of intermediate density, although less promising than high-density zones, may contain interesting mineralogical potential and merit further exploration.

Zones of high and very high lineament density are the most promising for mining exploration. These zones correspond to zones of intense fracturing, which have favored the concentration of minerals of economic interest. Lineament density analysis is a powerful tool for mineral exploration, it also has certain limitations. Rock fracturing is a complex phenomenon, influenced by many geological factors. Lineament density analysis alone cannot provide a complete picture of a site's geology. The results of density analysis must always be compared with field observations in order to validate interpretations and refine the geological understanding of the site.

Conclusion

The magnetic method has become a fundamental approach for investigating metal ores, enabling the direct mapping of deposits and a more comprehensive understanding of the complex geology that controls them. The application of advanced data processing techniques (first vertical derivative, analytical signal and Euler deconvolution) to high-resolution aeromagnetic data covering the Mandjap I zone revealed the presence of linear structures, intense magnetic anomalies and information on the depth and geometry of magnetic sources. The results of this study can be summarised as follows:

- The geological formations in the study area have undergone polyphase deformation.
- The statistical analysis of the lineaments revealed a specific distribution of their orientation along preferential directions including, ENE-WSW and NE-SW.
- These directions are characteristic of Pan-African tectonics on a regional scale and also correspond to the major Pan-African structures in Cameroon, namely the Central Cameroon Shear and the Sanaga Fault.
- Spectral analysis indicates a shallow magnetic basement of approximately 0.542 km.
- Zones with significant magnetic anomalies, in association with favourable geological structures, are priority targets for further exploration.

The results of this aeromagnetic survey provide a solid basis for further mineral exploration in the Mandjap I area. It would be interesting to conduct additional field campaigns such as surface geology, geochemistry and ground geophysics to validate and refine the identified targets. Targeted drilling could then be considered to evaluate the mineralization potential of the most promising zones.

References

1. Abdelrady M., Moneim M.A., Alarifi S.S., Abdelrady A., Othman A., Mohammed M.A. and Mohamed A., Geophysical investigations for the identification of subsurface features influencing mineralization zones, *Journal of King Saud University-Science*, **35**, 102809 **(2023)**

2. Abdelsalam M.G., Liégeois J.P. and Stern R.J., The saharan metacraton, *Journal of African Earth Sciences*, **34**, 119-136 **(2002)**

3. Abubakar F., Alao J.O., Ogah A.J., Ayuba R., Lekdukun M.O., Baba Y., Sadiq F.K., Samson E.E. and Aliyu A., Evaluation of gold mineralisation potential using AHP systems and weighted overlay analysis, *Scientific Reports*, **14**, 21263 **(2024)**

4. Adewumi T. and Salako K., Delineation of mineral potential zone using high resolution aeromagnetic data over part of Nasarawa State, North Central, Nigeria, *Egyptian Journal of Petroleum*, **27**, 759-767 **(2018)**

5. Akpa C., Nnabo P., Ani C., Obasi A., Obasi P. and Nworie C., Application of ground magnetic method for delineation subsurface structural control on sulphide ore deposit in Benue Trough; A Case Study of Ikenyi Izzi, *Earth Sci Malays*, **7**, 7-19 **(2023)**

6. Babu S.B., Satyakumar A., Kulkarni A.V. and Vats P.K., Structurally controlled mineralization in parts of Aravalli craton, India: Constraints from gravity and magnetic data, *Journal of Geodynamics*, **155**, 101954 **(2023)**

7. Blakely R.J., Potential theory in gravity and magnetic applications, Cambridge University Press **(1996)**

8. Cowan D. and Cowan S., Separation filtering applied to aeromagnetic data, *Exploration Geophysics*, **24**, 429-436 **(1993)**

9. Davis G.H., Bump A.P., García P.E. and Ahlgren S.G., Conjugate Riedel deformation band shear zones, *Journal of Structural Geology*, **22**, 169-190 **(2000)**

10. De Wit M., Stankiewicz J. and Reeves C., Restoring Pan-African-Brasiliano connections: more Gondwana control, less trans-Atlantic corruption, *Geological Society, London*, Special Publications, **294**, 399-412 **(2008)**

11. Dentith M. and Mudge S.T., Geophysics for the mineral exploration geoscientist, Cambridge University Press **(2014)**

12. Feumoe A.N.S., Ndougsa-Mbarga T., Manguelle-Dicoum E. and Fairhead J.D., Delineation of tectonic lineaments using aeromagnetic data for the south-east Cameroon area, *Geofizika*, **29**, 175-192 **(2012)**

13. Feybesse J., Johan V., Triboulet C., Guerrot C., Mayaga-Mikolo F., Bouchot V. and N'dong J.E., The West Central African belt: a model of 2.5–2.0 Ga accretion and two-phase orogenic evolution, *Precambrian Research*, **87**, 161-216 **(1998)**

14. Gazel J. and Gérard G., Carte géologique de reconnaissance du cameroun au 1/500 000, feuille Batouri-Est avec notice explicative, Mémoire, Direction Mines Géologie, Yaoundé Cameroun **(1954)**

15. Gérard A. and Griveau P., Interprétation quantitative en gravimétrie ou magnétisme à partir de cartes transformées de gradient vertical, *Geophysical Prospecting*, **20**, 459-481 **(1972)**

16. Hinze W.J., Von Frese R.R., Von Frese R. and Saad A.H., Gravity and magnetic exploration: Principles, practices and applications, Cambridge University Press **(2013)**

17. Jacobsen B.H., A case for upward continuation as a standard separation filter for potential-field maps, *Geophysics*, **52**, 1138-1148 **(1987)**

18. Kankeu B., Greiling R.O. and Nzenti J.P., Pan-African strike–slip tectonics in eastern Cameroon—Magnetic fabrics (AMS) and structure in the Lom basin and its gneissic basement, *Precambrian Research*, **174**, 258-272 **(2009)**

19. Leu L.K., Magnetic exploration with reduction of magnetic data to the equator, Google Patents **(1986)**

20. Leu L.K., Use of reduction-to-the-equator process for magnetic data interpretation, In Geophysics, Soc. Exploration Geophysicists 8801 S YALE ST, TULSA, OK 74137, **47**, 445-445 **(1982)**

21. Mono J.A., Bouba A., Amougou O.U.I.O., Ngoh J.D., Nyam F.M.E.A. and Mbarga T.N., Analysis of Aeromagnetic Data for Enhancing Geologic Features Using Filtering Techniques Over the Congo Craton–Pan-African Belt Contact, Centre-East Cameroon, *International Journal of Geophysics*, **2024**, 4767612 **(2024)**

22. Mushayandebvu M.F., van Driel P., Reid A.B. and Fairhead J.D., Magnetic source parameters of two-dimensional structures using extended Euler deconvolution, *Geophysics*, **66**, 814-823 **(2001)**

23. Nabighian M.N. and Hansen R., Unification of Euler and Werner deconvolution in three dimensions via the generalized Hilbert transform, *Geophysics*, **66**, 1805-1810 **(2001)**

24. Nabighian M.N. et al, The historical development of the magnetic method in exploration, *Geophysics*, **70**, 33ND-61ND **(2005)**

25. Ndema Mbongue J., Ngnotue T., Ngo Nlend C., Nzenti J. and Cheo Suh E., Origin and evolution of the formation of the Cameroon Nyong Series in the western border of the Congo Craton, *Journal of Geosciences and Geomatics*, **2**, 62-75 **(2014)**

26. Ndougsa-Mbarga T., Feumoe A.N.S., Manguelle-Dicoum E. and Fairhead J.D., Aeromagnetic data interpretation to locate buried faults in south-east Cameroon, *Geophysica*, **48**, 49-63 **(2012)**

27. Neves S.P. et al, Timing of crust formation, deposition of supracrustal sequences and Transamazonian and Brasiliano metamorphism in the East Pernambuco belt (Borborema Province, NE Brazil): implications for western Gondwana assembly, *Precambrian Research*, **149**, 197-216 **(2006)**

28. Neves S.P. Bruguier O. Vauchez A., Bosch D., Da Silva J.M.R. and Mariano G., Timing of crust formation, deposition of supracrustal sequences and Transamazonian and Brasiliano metamorphism in the East Pernambuco belt (Borborema Province, NE Brazil): implications for western Gondwana assembly, *Precambrian Research*, **149 (3-4)**, 197-216 **(2006)**

29. Nforba M.T., Api L., Berinyuy N. and Fils S.C.N., Advances in Remote Sensing and Geo Informatics Applications, eds. El-Askary Hesham M., Lee Saro, Heggy Essam and Pradhan Biswajeet, (Springer International Publishing, 197-201 **(2018)**

30. Ngako V., Affaton P. and Njonfang E., Pan-African tectonics in northwestern Cameroon: implication for the history of western Gondwan, *Gondwana Research*, **14**, 509-522 **(2008)**

31. Ngako V., Affaton P., Nnange J. and Njanko T., Pan-African tectonic evolution in central and southern Cameroon: transpression and transtension during sinistral shear movements, *Journal of African Earth Sciences*, **36**, 207-214 **(2003)**

32. Noutchogwe C.T., Koumetio F. and Manguelle-Dicoum E., Structural features of South-Adamawa (Cameroon) inferred from magnetic anomalies: Hydrogeological implications, *Comptes Rendus Geoscience*, **342**, 467-474 **(2010)**

33. Nzenti J.P., Kapajika B., Wörner G. and Lubala T.R., Synkinematic emplacement of granitoids in a Pan-African shear zone in Central Cameroon, *Journal of African Earth Sciences*, **45**, 74-86 **(2006)**

34. Nzenti J., Barbey P., Macaudiere J. and Soba D., Origin and evolution of the late Precambrian high-grade Yaoundé gneisses (Cameroon), *Precambrian Research*, **38**, 91-109 **(1988)**

35. Nzenti J., Njanko T., Njiosseu E.T. and Tchoua F., Les domaines granulitiques de la chaîne panafricaine Nord-Equatoriale au Cameroun, Geologie et Environnement au Cameroun, GEOCAM 1, 255-264 **(1998)**

36. Oliveira E., Toteu S., Araújo M., Carvalho M., Nascimento R., Bueno J., McNaughton N. and Basilici G., Geologic correlation between the Neoproterozoic Sergipano belt (NE Brazil) and the Yaoundé belt (Cameroon, Africa), *Journal of African Earth Sciences*, **44**, 470-478 **(2006)**

37. Owona S., Ondoa J.M., Ratschbacher L., Ndzana S.P.M., Tchoua F.M. and Ekodeck G.E., The geometry of the Archean, Paleo-and Neoproterozoic tectonics in the Southwest Cameroon, *Comptes Rendus Geoscience*, **343**, 312-322 **(2011)**

38. Penaye J., Toteu S., Tchameni R., Van Schmus W., Tchakounté J., Ganwa A., Minyem D. and Nsifa E., The 2.1 Ga West central

African belt in Cameroon: extension and evolution, *Journal of African Earth Sciences*, **39**, 159-164 **(2004)**

39. Pouclet A., Tchameni R., Mezger K., Vidal M., Nsifa E., Shang C. and Penaye J., Archaean crustal accretion at the northern border of the Congo Craton (South Cameroon): The charnockite-TTG link, *Bulletin de la Société Géologique de France*, **178**, 331-342 **(2007)**

40. Reeves C., Aeromagnetic surveys: principles, practice and interpretation, Vol. 155, Geosoft, Washington (DC) (**2005**)

41. Regnoult J.M., Synthèse géologique du Cameroun, Ministère des mines et de l'energie **(1986)**

42. Reid A.B., Allsop J., Granser H., Millett A.T. and Somerton I., Magnetic interpretation in three dimensions using Euler deconvolution, *Geophysics*, **55**, 80-91 **(1990)**

43. Reidel S.P., Saddle Mountains: the evolution of an anticline in the Yakima Fold Belt, *Am. J. Sci.*, **284(8)**, 942–978 **(1984)**

44. Roest W.R., Verhoef J. and Pilkington M., Magnetic interpretation using the 3-D analytic signal, *Geophysics*, **57**, 116-125 **(1992)**

45. Saha-Fouotsa A.N., Vanderhaeghe O., Barbey P., Eglinger A., Tchameni R., Zeh A., Tchunte P.F. and Nomo E.N., The geologic record of the exhumed root of the Central African Orogenic Belt in the central Cameroon domain (Mbé–Sassa-Mbersi region), *Journal of African Earth Sciences*, **151**, 286-314 **(2019)**

46. Saleh A. and Gabr S.S., Application of magnetic data and satellite spectral imaging in identifying gold mineralization zones and its associated subsurface structures at Fawakheir-Attala area, Central Eastern Desert, Egypt, *Environmental Earth Sciences*, **83**, 1-33 **(2024)**

47. Spector A. and Grant F., Statistical models for interpreting aeromagnetic data, *Geophysics*, **35**, doi.org:10.1190/1.1440092 **(1970)**

48. Thompson D., EULDPH: A new technique for making computer-assisted depth estimates from magnetic data, *Geophysics*, **47**, 31-37 **(1982)**

49. Toteu S.F., Penaye J. and Djomani Y.P., Geodynamic evolution of the Pan-African belt in central Africa with special reference to Cameroon, *Canadian Journal of Earth Sciences*, **41**, 73-85 **(2004)**

50. Toteu S., Van Schmus W., Penaye J. and Nyobe J., UPb and SmN edvidence for Eburnian and Pan-African high-grade metamorphism in cratonic rocks of southern Cameroon, *Precambrian Research*, **67**, 321-347 **(1994)**

51. Vacquier V., Interpretation of aeromagnetic maps, Vol. 47, Geological Society of America **(1954)**.

(Received 26th April 2024, accepted 04th July 2024)